

Al-SATURATED PHLOGOPITE: CHARGE CONSIDERATIONS AND CRYSTAL CHEMISTRY

THOMAS J. BUJNOWSKI¹, STEPHEN GUGGENHEIM^{1,*}, AND MARIA FRANCA BRIGATTI²

¹ Department of Earth and Environmental Sciences, University of Illinois at Chicago, Chicago, Illinois, 60607, USA

² Dipartimento di Scienze della Terra, Università di Modena e Reggio Emilia, Italy

Abstract—Factors controlling the crystal structure of phlogopite have been widely investigated; but the role of electrostatic interactions, for example, has received much less attention than other factors. The purpose of the present study was to perform a single-crystal refinement of an Al-saturated phlogopite and to use that refinement to supplement crystal-chemical analyses. The phlogopite investigated was from the Rumford quadrangle, Maine, and has the following chemistry: $(\text{K}_{0.81}\text{Na}_{0.03})_{\Sigma} = 0.84$ ($\text{Mg}_{1.84}\text{Fe}^{2+}_{0.52}\text{Al}_{0.45}\text{Mn}_{0.02}\text{Ti}^{4+}_{0.07}\right)_{\Sigma} = 2.90$ ($\text{Si}_{2.78}\text{Al}_{1.22}\right)_{\Sigma} = 4\text{O}_{10}(\text{OH}_{1.81},\text{F}_{0.05})_{\Sigma=1.86}$. The sample is a $1M$ polytype with $C2/m$ symmetry and cell dimensions of $a = 5.3220(4)$, $b = 9.2170(7)$, $c = 10.2511(8)$ Å, and $\beta = 100.081(1)$ °. Hydrogen atoms were located and the crystal structure was refined to give parameters $R_1 = 0.0301$ and weighted $R_2 = 0.0887$. The octahedral $M1$ site was larger than the $M2$ (average $M1-\text{O}$: 2.079 Å, average $M2-\text{O}$: 2.062 Å) and the electron counts were equal ($M1 = M2 = 14.8$ e⁻); based on bond distances, which are more accurate than electron counts in determining occupancy; this result is consistent with a slight preference of Mg for $M2$ and Fe^{2+} for $M1$.

Thirty-five Al-rich, natural phlogopite- $1M$ samples that are of (1) high metamorphic grade, and that have (2) total Al contents ≥ 1.27 atoms per formula unit (a.p.f.u.), (3) Fe^{3+} contents ≤ 0.11 a.p.f.u., and (4) Mn contents ≤ 0.10 a.p.f.u. along with the newly described phlogopite, exhibited crystal chemical trends related to increasing Al content. Octahedral substitutions of smaller, high-charge cations (*i.e.* Al) apparently decrease distortions in the octahedral sites and produce longer $M2-\text{O}_4$ distances. In addition, $\text{VI}^{\text{Fe}}\text{-F}$ avoidance apparently occurs in high Al-content samples, which are generally high in VI^{Fe} . The data set also shows that these samples have limited ordering among M sites (Fe^{2+} in $M1$ and Al in $M2$), an increase in β (99.96° to 100.32°) possibly caused by cation ordering and therefore size differences of $M1$ and $M2$, and interlayer (A) sites with $A-\text{O}_{\text{outer}}$ distances that increase and $A-\text{O}_{\text{inner}}$ distances that decrease with increasing Ti content.

Computer models were used to simulate electrostatic interactions in phlogopite structures with variable Al concentrations utilizing Pauling's electrostatic valency principle, which considers first-coordination electrostatic interactions. The model results were compared to the maximum Al concentrations in natural and synthetic phlogopite samples. Model results revealed no indications (*e.g.* a limit reached or a sudden change occurred) that charge saturation/undersaturation of the apical oxygen atoms at Al contents equal to the maximum in natural and/or synthetic samples causes instability that could not be balanced by bond-length variation. However, a cation of higher charge substituting at $M1$ (or $M2$) may result in higher electrostatic repulsions between the other octahedral sites. Thus, the Al^{3+} content in the octahedral sites may reach a maximum, with Fe^{2+} for Mg substitutions favored.

Key Words—Al-saturated Phlogopite, Electrostatic Modeling, Layer Charge, Crystal Chemistry, Single Crystal X-ray Diffraction, Refinement.

INTRODUCTION

Phlogopite, the trioctahedral Mg-rich end member of the biotite mica solid-solution series, has an ideal chemical formula of $\text{KMg}_3(\text{AlSi})_4\text{O}_{10}(\text{OH},\text{F})_2$. Trivalent Al may substitute for Mg^{2+} or for Si^{4+} , and where the latter occurs without the former, Al^{3+} is a contributor to the net layer negative charge. In equilibrated and most higher-temperature metamorphosed rocks, a maximum amount of Al substitution occurs by mechanisms involving bulk composition,

cation size, and/or effects of electrostatic charge. Many workers have investigated this Al-content maximum using synthetic and natural samples (Berman *et al.*, 2007; Crowley and Roy, 1964; Guidotti, 1984; Hewitt and Wones, 1975; Robert, 1976; Rutherford, 1973). Mercier *et al.* (2006) explored Al-saturation limits using geometric models and found limitations based on tetrahedral rotation. In contrast, electrostatic interactions have not previously been examined in detail, although cation size effects have been considered (Donnay *et al.*, 1964; Hewitt and Wones, 1975).

The purpose of the present study was to report a new structure refinement of a metamorphic phlogopite from an Al-saturated environment and to determine the maximum amount of Al substitution possible by examining charge substitutions and geometric para-

* E-mail address of corresponding author:
xtal@uic.edu
DOI: 10.1346/CCMN.2009.0570601

meters in metamorphosed phlogopite. In addition, the crystal chemistry was compared to other Al-saturated phlogopites from the literature.

EXPERIMENTAL

Sample and X-ray data collection

The phlogopite crystal, from rock sample Ru-P85s-75, used for X-ray analysis, is from the lower sillimanite zone of the Small Falls Formation located in the Rumford quadrangle in northwestern Maine. The assemblage (Guidotti, 1974; Guidotti *et al.*, 1975) is sillimanite + phlogopite + cordierite + muscovite + plagioclase(An40) + quartz + rutile + pyrrhotite + altered chlorite. Microprobe results of a phlogopite crystal from rock sample Ru-P85s-75 are presented (Table 1) and indicate a noticeable deficiency in interlayer cation occupancy, consistent with phlogopite from western Maine metamorphics (Guidotti *et al.*, 1988). Guidotti and Dyar (1991) speculated that $\text{X}^{\text{II}}(\text{K},\text{Na})^{+1}\text{X}^{\text{II}}(\text{H}_3\text{O})^{+}$ substitution (notation follows Burt, 1988) produces apparent interlayer vacancies in phlogopite from these rocks. Brigatti *et al.* (2008) correlated interlayer occupancy with interlayer size, which is in accord with this substitution.

Approximately 230 phlogopite crystals were examined using rotation frames (*i.e.* ‘photographs’) collected with a Bruker D8 SMART APEX system. An irregularly shaped crystal with approximate dimensions of 0.374 mm × 0.309 mm × 0.074 mm was chosen for detailed refinement after additional precession camera photographs were taken to verify that no reflections were diffuse. Single-crystal X-ray data collection was performed using monochromatized MoK α radiation (0.7107 Å). A collimator aperture size of 0.5 mm was used, and data were collected using a frame-time exposure of 25 s on a CCD detector with 1024×1024 pixel resolution and a crystal-to-detector distance of 60 mm. An initial unit-cell determination using three sets of 20 frames collected at 10 s each resulted in a C-centered cell. The unit-cell refinement involved SMART (Bruker, 2007) for data collection and data reduction and integration involved SAINT (Bruker, 2007). The unit-cell parameters are: $a = 5.3220(4)$, $b = 9.2170(7)$, $c = 10.2511(8)$ Å, and $\beta = 100.081(1)$. A Gaussian absorption correction was performed using a linear absorption coefficient (μ) of 1.90 mm^{-1} . The absorption correction, space-group determination, and data merging were performed using XPREP, part of the SHELXTL software package (Sheldrick, 1997).

Refinement

The initial atomic parameters for refinement were obtained from oxybiotite-1M (Ohta *et al.*, 1982). An idealized phlogopite chemical composition was used for most refinement cycles, but final cycles included the composition determined by microprobe analysis. Site

refinement indicated that the electron count (14.8 e^-) of $M1$ was equal to that of $M2$. When the R_1 value ($R_1 = \Sigma|F_o| - |F_c|/\Sigma|F_o|$) reached 0.035, F and OH were included in the O4 site. Refinement was based on F_o^2 and weighted $R_2 = \{\Sigma[w(F_o^2 - F_c^2)^2]/\Sigma[w(F_o^2)^2]\}^{1/2}$. The weighting scheme used during the refinement was defined as: weight (w) = $1/[\sigma^2(F_o^2) + (aP)^2 + bP]$, where P is $(F_o^2 + 2F_c^2)/3$ and a and b are refined. Initial values were set at $a = 0.1$ and $b = 0$, and the values refined to $a = 0.0556$ and $b = 0.3020$ for the final cycle. At the end of the refinement, hydrogen atoms were found by Fourier difference synthesis. The difference peak associated with O4 yielded the smallest R_1 factor (0.031) and is consistent with hydrogen. The O4–H vector [distance of $1.00(7)$ Å] forms an angle of 90° from the (001). Because of the abundance of collected data, twelve $00l$ reflections that poorly matched to calculated values were removed before the final refinement cycle to increase precision, resulting in a total of 640 reflections. The final refined parameters are: $R_1 = 0.0301$ for $616 F_o > 4\sigma(F_o)$ reflections, 0.0309 for all 640 reflections, weighted $R_2 = 0.0887$, and goodness-of-fit = 1.270.

Electrostatic modeling

Models of 2:1 phlogopite layers were computer simulated using Matlab software (MathWorks, 2006) to monitor the Pauling bond strength (PBS) at each apical oxygen, and thus the modeling concerns first-coordination electrostatic interactions only. The PBS is the total electrostatic charge that an atom receives from each of its nearest neighbors divided by the coordination number. For example, in an ideal structure, the nearest neighbors of an apical oxygen atom are three octahedral R^{2+} cations and a tetrahedral Si^{4+} cation, which causes the apical oxygen atom to experience a combined charge

Table 1. Microprobe analysis of phlogopite, Ru-P85s-75.

Oxide	Wt.%	Atoms	
SiO ₂	38.64	Si	2.78
Al ₂ O ₃	19.61	^{IV} Al	1.22 } 4.00
MgO	17.11		
FeO	8.62	^{VI} Al	0.45
MnO	0.36	Mg	1.84
TiO ₂	1.27	Fe ²⁺	0.52 } 2.90
Cr ₂ O ₃	0.04	Mn	0.02
K ₂ O	8.83	Ti	0.07
Na ₂ O	0.19	Cr	0.002
BaO	0.09		
		K	0.81
H ₂ O	3.73	Na	0.03 } 0.84
		Ba	0.003
F	0.91		
Total	99.39	OH	1.81 } 1.86
		F	0.05

Microprobe analysis performed by M. Yates, University of Maine, USA.

Table 2. Atomic coordinates and displacement parameters.

Atom	<i>x</i>	<i>y</i>	<i>z</i>	<i>U</i> _{eq} *	<i>U</i> ₁₁	<i>U</i> ₂₂	<i>U</i> ₃₃	<i>U</i> ₁₂	<i>U</i> ₁₃	<i>U</i> ₂₃
<i>A</i>	0.0	0.5	0.0	0.0331(3)	0.0318(6)	0.0324(6)	0.0351(6)	0.0	0.0062(5)	0.0
<i>M1</i>	0.0	0.0	0.5	0.0125(3)	0.0099(4)	0.0099(5)	0.0183(5)	0.0	0.0039(3)	0.0
<i>M2</i>	0.0	0.33246(6)	0.5	0.0133(2)	0.0097(4)	0.0119(4)	0.0184(4)	0.0	0.0027(3)	0.0
<i>T</i>	0.07622(9)	0.16694(4)	0.22794(5)	0.0110(2)	0.0086(3)	0.0087(3)	0.0159(3)	-0.0001(1)	0.0028(2)	-0.0000(1)
O1	0.0093(4)	0.0	0.1718(2)	0.0224(4)	0.0264(9)	0.0160(9)	0.0237(9)	0.0	0.0010(7)	0.0
O2	0.3306(2)	0.2264(2)	0.1710(1)	0.0219(3)	0.0188(6)	0.0250(8)	0.0230(7)	-0.0068(5)	0.0065(5)	-0.0029(5)
O3	0.1320(3)	0.1679(1)	0.3927(1)	0.0159(3)	0.0154(7)	0.0158(8)	0.0168(7)	0.0004(4)	0.0032(5)	0.0000(4)
O4	0.1300(4)	0.5	0.3991(2)	0.0191(4)	0.0168(9)	0.0210(9)	0.0195(9)	0.0	0.0030(7)	0.0
H	0.10(1)	0.5	0.300(7)	0.13(2)						

Displacement parameters of the form: $\exp[-2\pi^2(U_{11}h^2\mathbf{a}^{\ast 2} + U_{22}k^2\mathbf{b}^{\ast 2} + U_{33}l^2\mathbf{c}^{\ast 2} + 2U_{12}hka^*\mathbf{b}^* + 2U_{13}hla^*\mathbf{c}^* + 2U_{23}k/b^*\mathbf{c}^*)]$

* Isotropic equivalent displacement factor

of 2.0 [= 3*(2/6) + 1*(4/4)]. This is equal to the formal charge of the anion, but opposite in sign. As the Al concentration increases, some apical oxygen atoms experience a charge summation that reflects an oversaturation or undersaturation in electrostatic charge (Guggenheim *et al.*, 1987). These deviations in charge can be compensated by an adjustment in bond lengths (Brown, 1992) though not in the present case where electrostatic modeling calculations of PBS were not included in the models to simplify the programming effort. In the modeled layers, the number of octahedral vacancies and the number of Al cations were varied for the octahedral and tetrahedral sites. The models assumed that Al-substituted tetrahedral sites cannot occupy two corner-sharing tetrahedra (Loewenstein, 1954) and that the space group was of *C2/m* or lower symmetry.

Tetrahedral sheets were generated following Lee *et al.* (2007) where Al was randomly dispersed. Octahedral sheets were generated by randomly dispersing Al or vacancies in the *M* sites in fixed amounts. Each model run contained ~ 360,000 tetrahedra per layer. The PBS was monitored and its value recorded for each apical oxygen atom as the number of Al cations and vacancies varied.

RESULTS

Refinement

The final atomic coordinates and displacement parameters are listed in Table 2, calculated bond lengths and angles in Table 3, and structural parameters in Table 4. A comparison of ideal ionic radii (Shannon, 1976) and

Table 3. Selected calculated bond lengths (Å) and angles (°).

Tetrahedral

<i>T</i> –O2	1.658(1)			About <i>T</i>	
–O2'	1.658(1)	O1–O2'	2.695(2)	108.64(8)	
–O1	1.660(1)	–O2	2.699(2)	108.86(9)	
–O3	1.663(1)	–O3	2.726(2)	110.26(8)	
Average:	1.660	O2–O2'	2.696(1)	108.80(8)	
		–O3	2.723(1)	110.12(6)	
		O3–O2'	2.722(2)	110.11(6)	

		Interlayer
<i>A</i> –O1 (× 2)		2.962(2)
–O2 (× 4)		2.965(2)
–O2 (× 4)		3.384(2)
–O3 (× 2)		3.396(2)
Average inner:		2.964
Average outer:		3.388

Octahedral

		<i>M2</i>	
<i>M1</i>			<i>M2</i> –OH (× 2)
<i>M1</i> –OH (× 2)	2.058(2)		2.046(1)
<i>M1</i> –O3 (× 4)	2.090(1)		<i>M2</i> –O3 (× 2)
Average:	2.079		2.068(1)
			<i>M2</i> –O3 (× 2)
			2.072(1)
		Average:	2.062
Unshared			Unshared
O3–OH (× 4)	3.060(2)	O3–OH (× 4)	O3–O3' (× 2)
–O3 (× 2)	3.095(1)	–O3 (× 2)	–OH (× 2)
Average:	3.072	Average:	3.062(2)
			<i>O3</i> –O3
			2.810(2)
			–O3' (× 2)
			2.783(2)
			OH–O3' (× 2)
			2.758(2)
			–OH
			2.683(3)
		Average:	3.061
			Average:
			2.763

Table 4. Observed structural parameters for phlogopite, Ru-P85s-75.

Parameter	Value
α_{Tet} (°)	9.35
τ_{Tet} (°)	110.16
Ψ (°)	K M1 M2 Mean M1,M2
β_{ideal} (°)	59.64 59.64 59.36 59.50 99.97
Sheet thickness (Å)	Tetrahedral $\times 2$ Octahedral Interlayer separation Total $c \sin \beta$
Δz_{ave} (Å)	4.534 2.102 3.457 10.093 10.093* 0.0038

* Provided to facilitate comparison with total.

Note: structural parameters are as defined by Bailey (1984).

observed $M-\text{O}_2\text{OH}$ bond lengths indicates an octahedral chemistry of $M1 = \text{Mg}_{0.47}\text{Fe}_{0.32}^{2+}\text{Al}_{0.15}\text{Ti}_{0.02}\text{Mn}_{0.02}$ (a.p.f.u.) and $M2 = \text{Mg}_{0.75}\text{Fe}_{0.04}^{2+}\text{Al}_{0.15}\text{Ti}_{0.02}\text{Mn}_{0.02}$ (a.p.f.u.), assuming only Fe^{2+} (no ferric iron) is present. Vacancies, Al, Ti, and Mn were equally distributed among $M1$ and $M2$. These site assignments should not be considered a unique solution. Microprobe chemical analysis, which was not performed on the grain used for X-ray study, indicates a larger total M -site electron count

(62.1 e⁻) than the occupancy refinement (44.3 e⁻) and bond-distance derived results (42.6 e⁻); this is attributed to chemically inhomogeneous phlogopite grains within the rock sample.

Electrostatic calculations

The metamorphosed samples with a bulk chemical composition that was high in Al and presumably Al-saturated were considered. Sufficient deviation of the charge of the apical oxygen atoms from a balanced charge was assumed to be potentially destabilizing. Therefore, the goal of the modeling process was to identify models containing a large number of apical oxygen atoms that are either undersaturated or oversaturated with respect to charge.

Results are shown in selected plots (Figure 1) to demonstrate the progression of the modeling. In the plots, the percentage of the apical oxygen atoms (with a given PBS) vs. the range in PBS (as defined in the caption) are plotted as a function of Al and vacancy ratios (vacancies set to zero in the selected plots). Eight PBS values are possible for each apical oxygen atom where no vacancies are present (Table 5), but many more values appear when vacancies are considered. Undersaturation of bond strength at ≤ 1.40 was considered an extreme case and unlikely to occur because two or more vacancies are required in adjacent octahedral sites.

Most phlogopite samples (Table 6) were selected from the literature based on: (1) high metamorphic grade (assumes equilibrated conditions), (2) total Al content

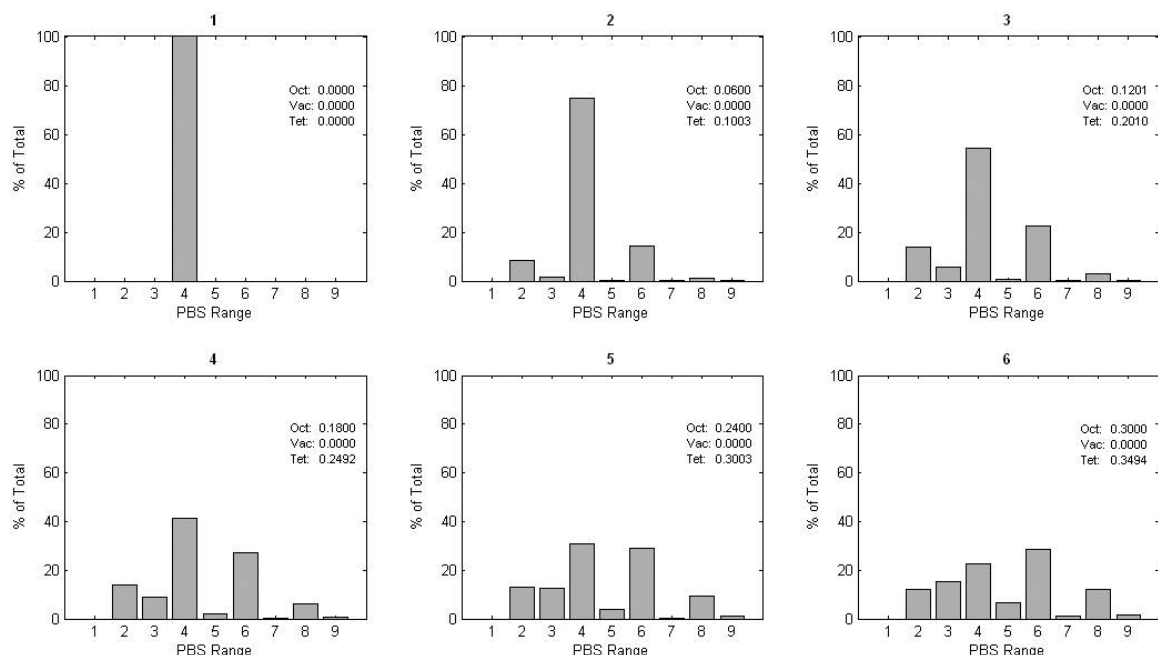


Figure 1. Plots showing the percentage of total apical oxygen atoms vs. PBS experienced by apical oxygen atoms where vacancies are at zero and octahedral and tetrahedral Al are varied. Al concentrations are per 4 tetrahedral sites/formula unit and per 3 octahedral sites/formula unit. The PBS ranges are separated as follows: (1) < 1.75, (2) 1.75, (3) 1.916, (4) 2.00, (5) 2.083, and (6) 2.16.

Table 5. Possible charge configurations of one tetrahedral cation (T) and three octahedral cations (M_1 , M_2 , M_3) surrounding an apical oxygen atom and the corresponding PBS for that oxygen atom.

T	M_1	M_2	M_3	PBS	T	M_1	M_2	M_3	PBS
4	3	3	3	2.5000	3	3	3	0	1.7500*
4	3	3	2	2.3333	4	2	2	0	1.6667*
3	3	3	3	2.2500	3	2	3	0	1.5833*
4	2	3	2	2.1667	3	2	2	0	1.4167*
3	3	3	2	2.0833	4	3	0	0	1.5000*
4	3	3	0	2.0000*	4	2	0	0	1.3333*
4	2	2	2	2.0000	3	3	0	0	1.2500*
3	2	3	2	1.9167	3	2	0	0	1.0833*
4	2	3	0	1.8333*	4	0	0	0	1.0000*
3	2	2	2	1.7500	3	0	0	0	0.7500*

* PBS configurations which contain vacancies.

≥ 1.27 atoms per formula unit (a.p.f.u.), (3) Fe^{3+} content ≤ 0.11 a.p.f.u., and (4) Mn content ≤ 0.10 a.p.f.u.. From these data, the greatest Al content found in natural samples was 0.345 per four tetrahedral sites per formula unit and 0.213 per three octahedral sites per formula unit. The greatest number of vacancies was 0.057 vacancies per three octahedral sites per formula unit.

Guidotti (1984) plotted a comprehensive list of amphibolite-grade biotite samples and found that VIAl is restricted to between 0 and 0.5 atoms per 11 oxygen atoms. Al-saturated synthetic samples were reported by Hewitt and Wones (1975) and Robert (1976). Samples synthesized with maximum Al contents were $\text{KMg}_{2.25}\text{Al}_{0.75}(\text{Al}_{1.75}\text{Si}_{2.25})\text{O}_{10}(\text{OH})_2$ (Hewitt and Wones, 1975), and $\text{KMg}_{2.01}\text{Al}_{0.813}(\text{Al}_{1.4625}\text{Si}_{2.54})\text{O}_{10}(\text{OH})_2$ at 600°C and $\text{KMg}_{2.5}\text{Al}_{0.375}(\text{Al}_{1.125}\text{Si}_{2.875})\text{O}_{10}(\text{OH})_2$ at 800°C (Robert, 1976). Crowley and Roy (1964) reported a chemistry of $\text{KMg}_2\text{Al}_1(\text{Al}_2\text{Si}_2)$

$\text{O}_{10}(\text{OH})_2$ determined from shifts in cell parameters and phases present in melts. Other Al-saturated samples have been synthesized and studied (e.g. Rutherford, 1973; and more recently, Berman *et al.*, 2007), but all are within the Al content range presented by Hewitt and Wones (1975) and Robert (1976), and therefore were not included here. Synthetic samples have greater Al contents than natural samples.

At the maximum Al content of the natural samples with no vacancies, the apical oxygen atoms that have a PBS of 2.0 are ~32% of the total (obtained in the same manner as percentages from Figure 1). Not surprisingly, increasing octahedral Al produces a greater number of models with apical oxygen atoms having PBS values of >2.0 , and increasing tetrahedral Al increases the number of models with apical oxygen atoms having PBS values of <2.0 . Models yielding PBS values for the apical oxygen atoms in the first range, or <1.75 , occur where

Table 6. List of natural samples used in this study.

Publication	Sample	Publication	Sample
Brigatti <i>et al.</i> (1991)	s15	Laurora <i>et al.</i> (unpublished)	6B
Brigatti <i>et al.</i> (2005)	AA3	Laurora <i>et al.</i> (unpublished)	BP1
Schingaro <i>et al.</i> (2005)	BHG1	Laurora <i>et al.</i> (unpublished)	BP34c
Laurora <i>et al.</i> (2007)	MS3(2)	Alietti <i>et al.</i> (1995)	phl1a
Laurora <i>et al.</i> (2007)	MS3(1)	Alietti <i>et al.</i> (1995)	phl1b
Brigatti <i>et al.</i> (2005)	AA4	Brigatti <i>et al.</i> (2005)	CA1
Brigatti <i>et al.</i> (2005)	CC	Brigatti <i>et al.</i> (2005)	CA2
Laurora <i>et al.</i> (unpublished)	BP21	Brigatti <i>et al.</i> (2000)	A4
Brigatti <i>et al.</i> (1991)	s8	Brigatti <i>et al.</i> (2008)	O-K-9
Laurora <i>et al.</i> (unpublished)	Bp34s	Brigatti <i>et al.</i> (2008)	O-C-30
Laurora <i>et al.</i> (unpublished)	A8	Brigatti <i>et al.</i> (2000)	H87
Brigatti <i>et al.</i> (2005)	5D	Brigatti <i>et al.</i> (2008)	O-K-47
Laurora <i>et al.</i> (2007)	MS9_I	Brigatti <i>et al.</i> (2008)	O-J-67
Laurora <i>et al.</i> (unpublished)	BP38	Brigatti <i>et al.</i> (2000)	C3-31
Brigatti <i>et al.</i> (1991)	s17	Brigatti (unpublished)	C6b
Laurora <i>et al.</i> (unpublished)	BP37	Brigatti <i>et al.</i> (2000)	GFS15a
Laurora <i>et al.</i> (2007)	MS5	Brigatti <i>et al.</i> (2000)	B1
This study	Ru-P85s-75	Brigatti <i>et al.</i> (2000)	CC1

no octahedral Al is present but vacancies exist. The percentage of apical oxygen atoms that showed a PBS value of 2.5 (Figure 1, range 9) and/or 2.25 (Figure 1, range 7) rarely occurred in the models and PBS of 2.333 (~7% on average at the Al maximum in natural samples) increased as Al was added to the octahedral sites of the models and decreased slowly as Al was added to tetrahedral sites. The configurations showing a PBS of 1.75 (Figure 1, range 2) were numerous (~17% on average at the Al maximum in natural samples).

DISCUSSION

Refinement and natural samples

The crystal chemistry of natural Al-rich phlogopite samples (Table 6) was analyzed along with the structure refined in this study. Octahedral distortion parameters were used to determine how Al substitution affects the phlogopite structure. The amount of distortion of the octahedral sites was calculated using the variance of the M –O distances. Where distortion was compared to ^{VI}Al ($M1$ in Figure 2a and $M2$ in Figure 2b), $M2$ exhibited a stronger trend than $M1$; and they both exhibited a steady decrease in distortion above 0.20 ^{VI}Al a.p.f.u.. An overall decrease in distortion might be expected considering that smaller, high-charge cations generally produce strong M –O bonds and a more regular octahedron if all the anions are the same species and if they are electrostatically balanced.

Variation in the $M2$ –O4 (O4 is the oxygen of the hydroxyl) distance had a large effect on the distortion of $M1$ (Figure 3a) and $M2$ (Figure 3b) and, in both cases, the amount of distortion decreased as $M2$ –O4 bonds became longer and less susceptible to variability about an octahedron (assuming anions are of the same species and are electrostatically balanced). Thus, plots of high-charged octahedral cations *vs.* $M2$ –O4 distances

(Figure 3c) revealed that an increase in the amount of high-charged cations in octahedral sites produced less distortion in both sites.

An increase in $M1$ –O distances with increasing Fe^{2+} (Figure 4a) and no correlation between $M2$ –O distances and Fe^{2+} (Figure 4b) suggested limited ordering among M sites with a preference of Fe^{2+} for $M1$. The influence of Al on the topology of $M2$ and the effect of Fe^{2+} on $M1$ –O distances suggest that Al is ordered to $M2$ and Fe^{2+} to $M1$. In Al-rich 1M biotites, Brigatti *et al.* (2000) found that ^{VI}Al is mostly in $M2$ sites and Fe^{2+} is mostly in $M1$ sites, consistent with the results here. The shared O3–O3' edge between two $M2$ sites also indicated that at an Al content of ~1.5 a.p.f.u. Al significantly affected the shared edge of the $M2$ sites and that cation-cation repulsions decreased the length of the shared edges (Figure 5).

In contrast to the present study, Brigatti *et al.* (2000) studied Al-saturated 1M biotites and found that the octahedral angle variance (OAV; Robinson *et al.*, 1971), as a measure of distortion, increased in both $M1$ and $M2$ sites with increasing ^{VI}Al content and that $M1$ showed the greater distortion. The results from the present study covered a larger range of samples and demonstrated that, in each octahedral distortion plot (Figure 2a,b), the range of distortion of $M1$ is smaller than the range of $M2$ and that $M2$ becomes more regular than $M1$ at greater Al concentrations. This suggests that, as Al increases, the $M2$ site becomes less distorted, whereas the $M1$ site is unaffected. Brigatti *et al.* (2000) also demonstrated that 1M biotites have shorter mean $M2$ –O distances resulting primarily from a reduction in $M2$ –O3 bond lengths with increasing ^{VI}Al content and that the octahedral thickness was reduced as ^{VI}Al increased. In the present study, a general decrease in $M2$ –O3 bond lengths (Figure 6a) (similar to Brigatti *et al.*, 2000) was observed and no apparent trend exists between octahedral thickness and ^{VI}Al (Figure 6b) (unlike Brigatti *et al.*, 2000). The lack

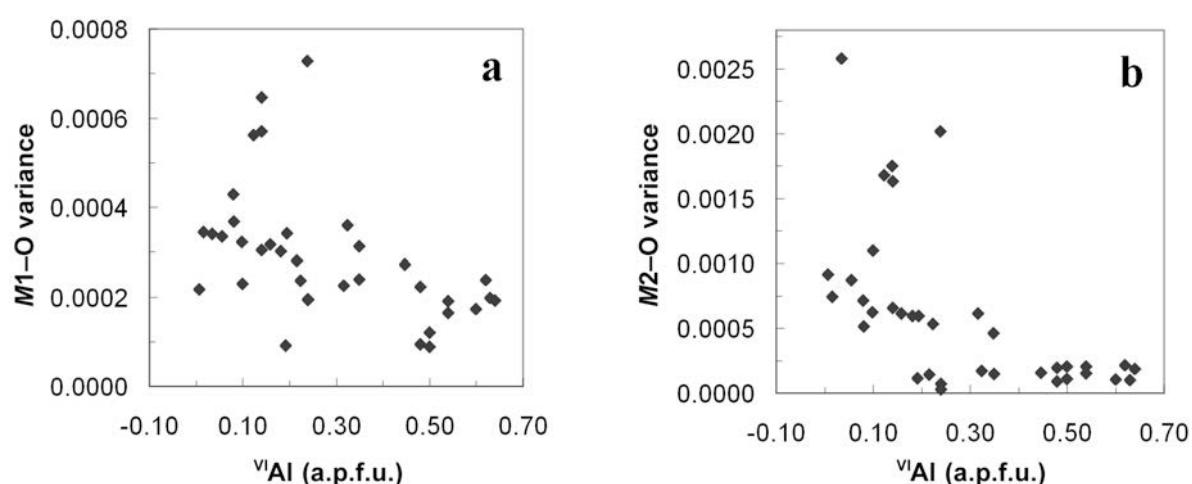


Figure 2. ^{VI}Al *vs.* the variance of M –O bond lengths of $M1$ (a) and $M2$ (b).

of such an apparent trend may be a result of a lack of precision.

In addition, in the Al-rich 1M biotites, Brigatti *et al.* (2000) found that the difference between M1 unshared

and shared edge lengths ($U_{M1} - S_{M1}$) increased with ^{VI}Al (Figure 7a) and with $\text{Fe}^{2+}/(\text{Fe}^{2+} + \text{Mg})$ (Figure 7b) thereby indicating that M1 distortion was controlled by M1 and M2 cation ordering. This ordering between the M1 and M2 sites has the effect of reducing the length of shared edges and enlarging unshared edges. In the present data set, no significant increase in $U_{M1} - S_{M1}$ was observed when compared to ^{VI}Al or $\text{Fe}^{2+}/(\text{Fe}^{2+} + \text{Mg})$ and less distortion of the M1 site occurred as ^{VI}Al increased.

A structural distortion observed in dioctahedral micas but not in trioctahedral micas is the relationship between β and the size of the M1 site (Bailey, 1984). An increase in the size of M1, attributed to vacancies in dioctahedral micas, causes a larger diagonal edge of the *trans* M1 octahedron, a larger intralayer shift, and consequently an increase in β . Presumably, a sufficient difference in size

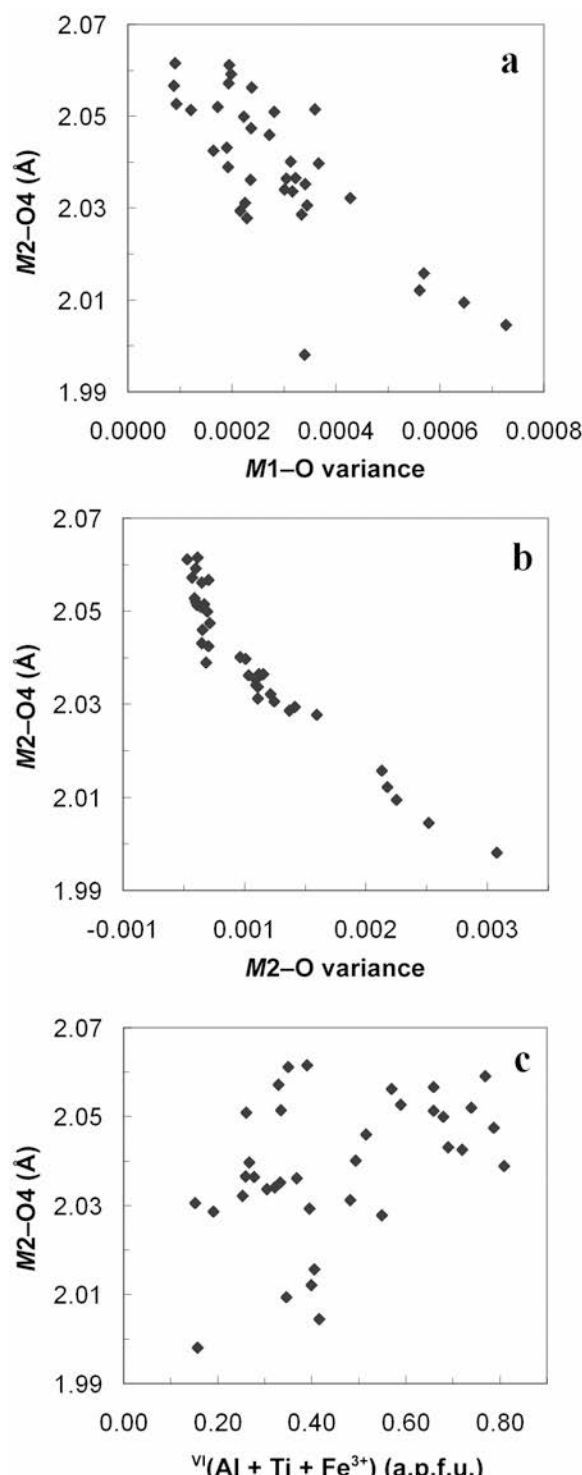


Figure 3. Variability of $M2-\text{O}4$ bond lengths in M1 (a) and M2 (b). (c) Mean $M2-\text{O}4$ vs. $\text{Al} + \text{Ti} + \text{Fe}^{3+}$ in six-fold coordination.

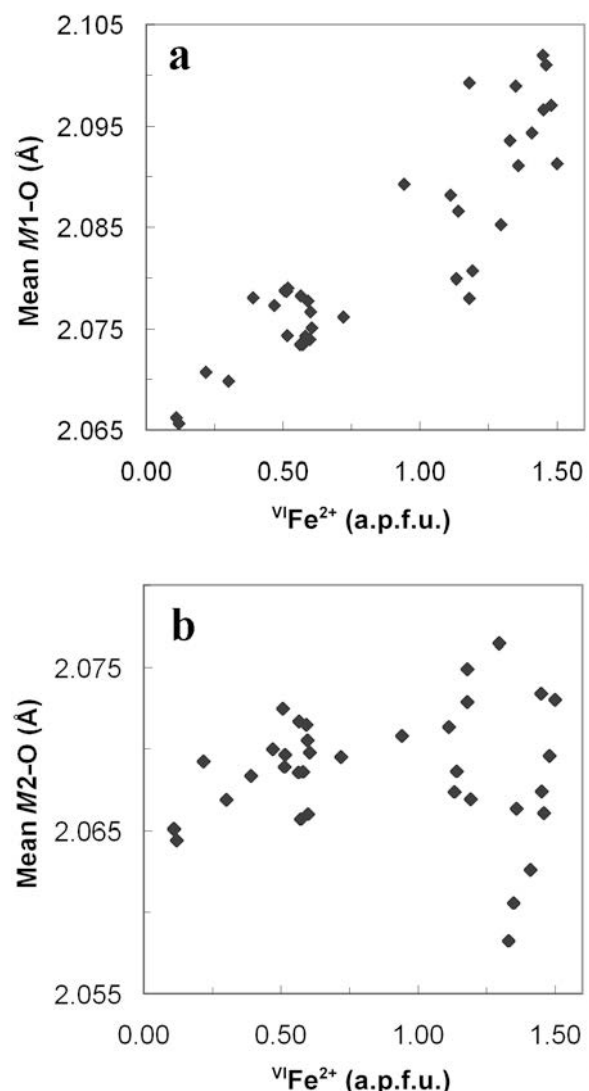


Figure 4. (a) Fe^{2+} vs. mean $M1-\text{O}$ and (b) $M2-\text{O}$ distances.

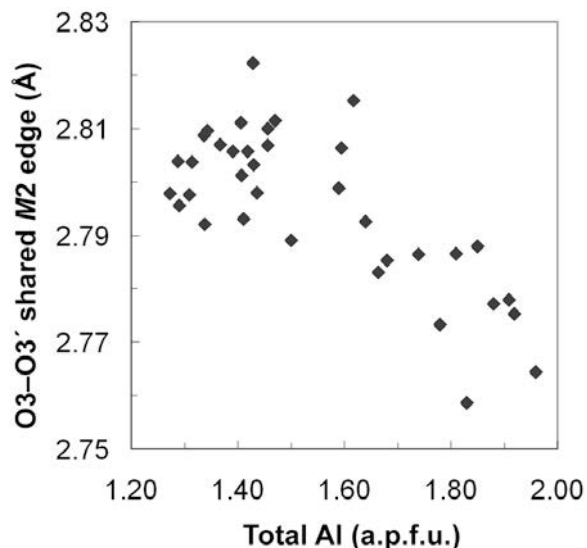


Figure 5. Total Al vs. O₃–O_{3'} shared edge between M₂ sites.

of the M₁ and M₂ octahedra in trioctahedral micas would also cause a shift in β . In the present sample set, a size difference between M₁ and M₂ exists which apparently causes an increase in β (99.96° to 100.32°) (Figure 8a). This phenomenon is probably related to cation ordering; see, for example, where ^{VI}Ti⁴⁺O₂²⁻^{VI}Mg²⁺(OH)₂⁻] and the concomitant deprotonation of the O₄ site in micas along the phlogopite–annite join caused the interlayer cation to move deeper into the interlayer cavity. The interlayer charge saturation by the O₄ site would be expected to

Brigatti and Guggenheim (2002) found that ‘Ti-oxy’ substitution [^{VI}Ti⁴⁺O₂²⁻^{VI}Mg²⁺(OH)₂⁻] and the concomitant deprotonation of the O₄ site in micas along the phlogopite–annite join caused the interlayer cation to move deeper into the interlayer cavity. The interlayer charge saturation by the O₄ site would be expected to

cause an increase in A–O_{outer} distances though this was not found in the samples in the present study (Figure 9a). An increase in Ti content is accompanied by a decrease in the *c* axis dimension (Figure 9b), A–O_{outer} distances decrease, and A–O_{inner} distances increase (Figure 9c) with one outlier observed (Brigatti, unpublished sample O-K-9). These changes are probably related to the small size of Ti with a reduction in the size of the octahedral sheet and compensating effects of the rotation angle to allow the tetrahedral sheet to mesh with the octahedral sheet.

Electrostatic modeling (first-coordination interactions)

The idea of the modeling was to see how substitutions of Al could result in the electrostatic unbalancing of the apical oxygen atom. Ignoring vacancies, PBS values of 2.5 and 2.25 required three or four Al cations in adjacent octahedra and tetrahedra, and this is an unlikely configuration because three Al occupying adjacent edge-sharing octahedra would result in cation–cation repulsions (second-coordination interactions). Thus, PBS values of 2.5 and 2.25 involve unlikely Al configurations in phlogopite. PBS values of 2.166, 2.0833, and 1.9166 are neither sufficiently charge oversaturated nor undersaturated to produce a relatively unstable structure as bond-distance adjustments can easily compensate. PBS values of 2.333 and 1.75 indicate significant charge imbalance; Al configurations that produce such values may lead to a relatively unstable structure, depending on the number of occurrences of this configuration in the structure.

In models involving octahedral vacancies, configurations containing Si in the tetrahedral site and two Al and a vacancy in the octahedral sites produce a PBS value of 2.0 and would add to the relative stability of the structure. Other configurations (as indicated in

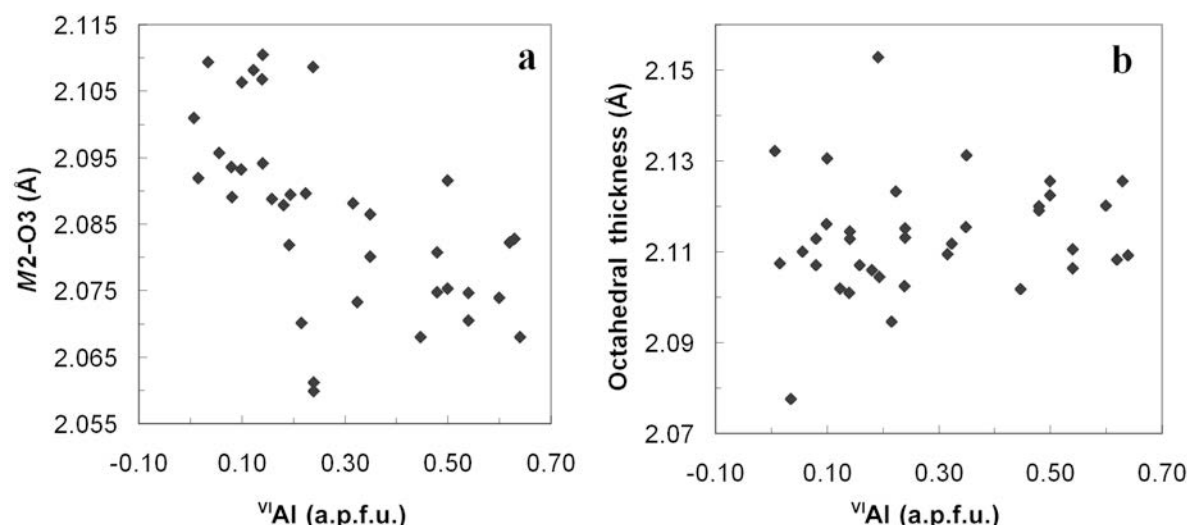


Figure 6. (a) ^{VI}Al vs. M₂–O₃ distance and (b) octahedral thickness.

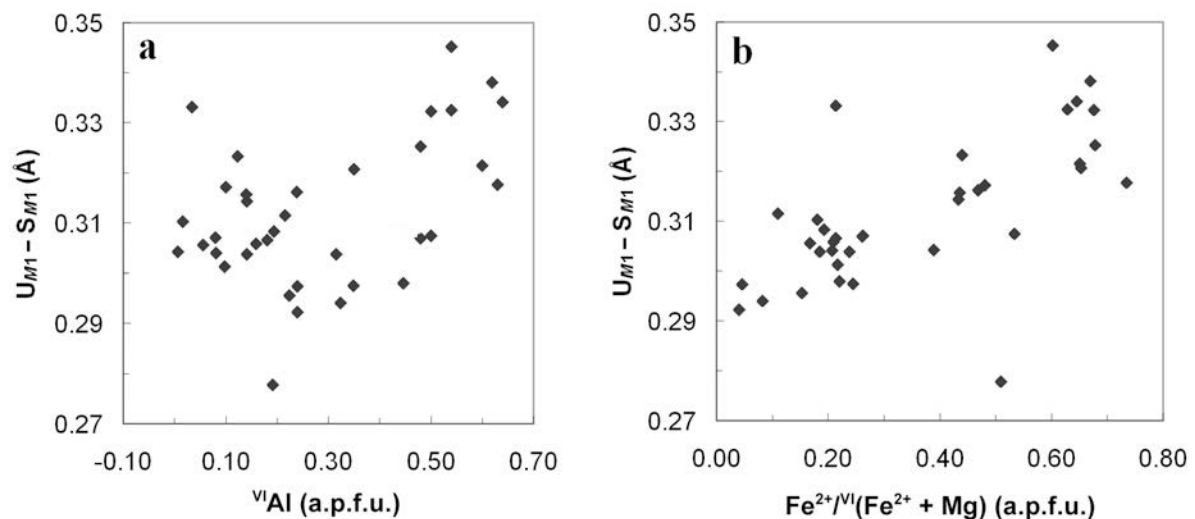


Figure 7. (a) The difference between unshared and shared M_1 edges ($U_{M1} - S_{M1}$) vs. $v^I\text{Al}$ and (b) $\text{Fe}^{2+}/v^I(\text{Fe}^{2+} + \text{Mg})$.

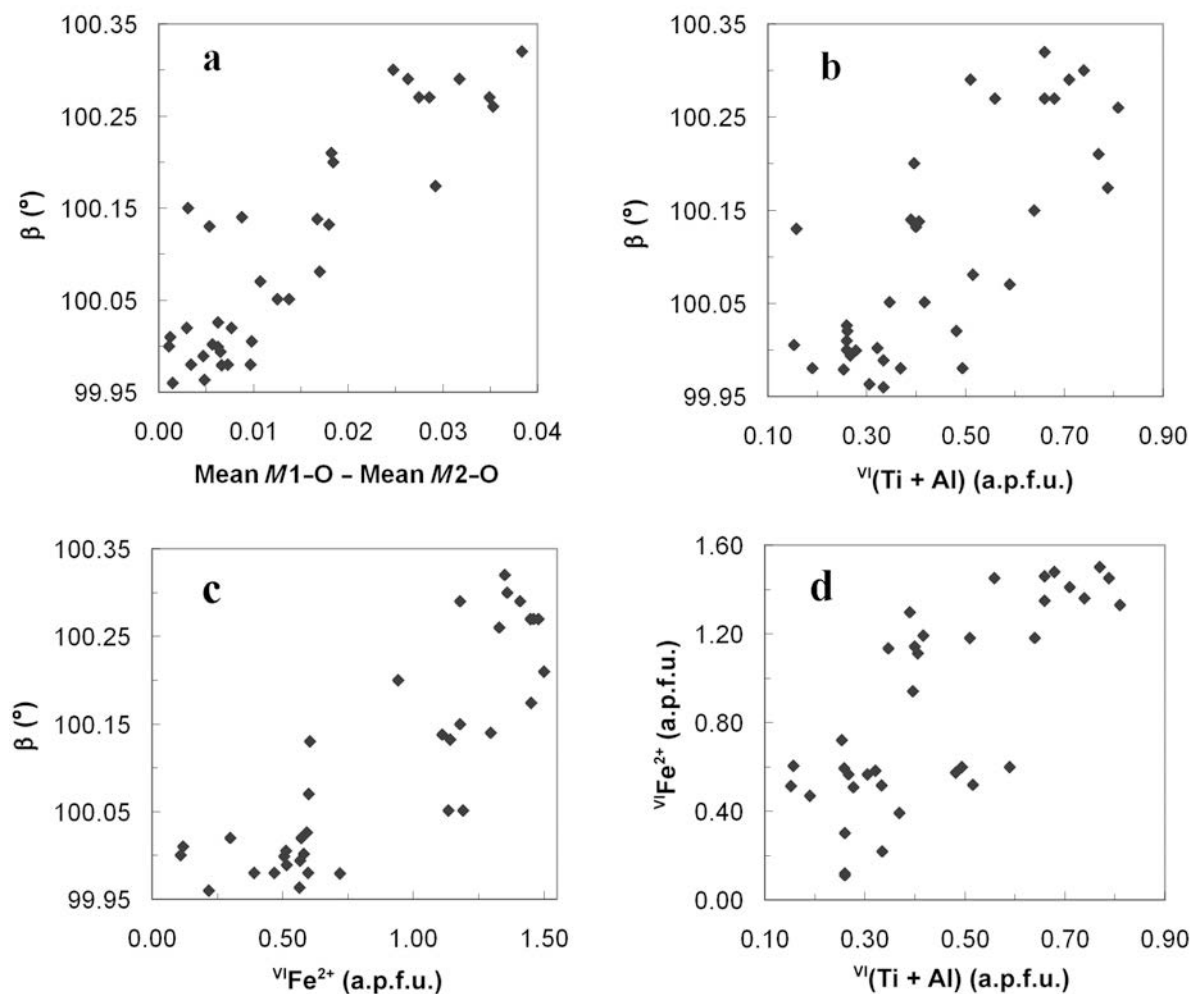


Figure 8. (a) β vs. the difference of mean $M1-O$ and mean $M2-O$ distances, (b) $v^I(\text{Ti} + \text{Al})$, (c) $v^I\text{Fe}^{2+}$, and (d) $v^I(\text{Ti} + \text{Al})$ vs. Fe^{2+} .

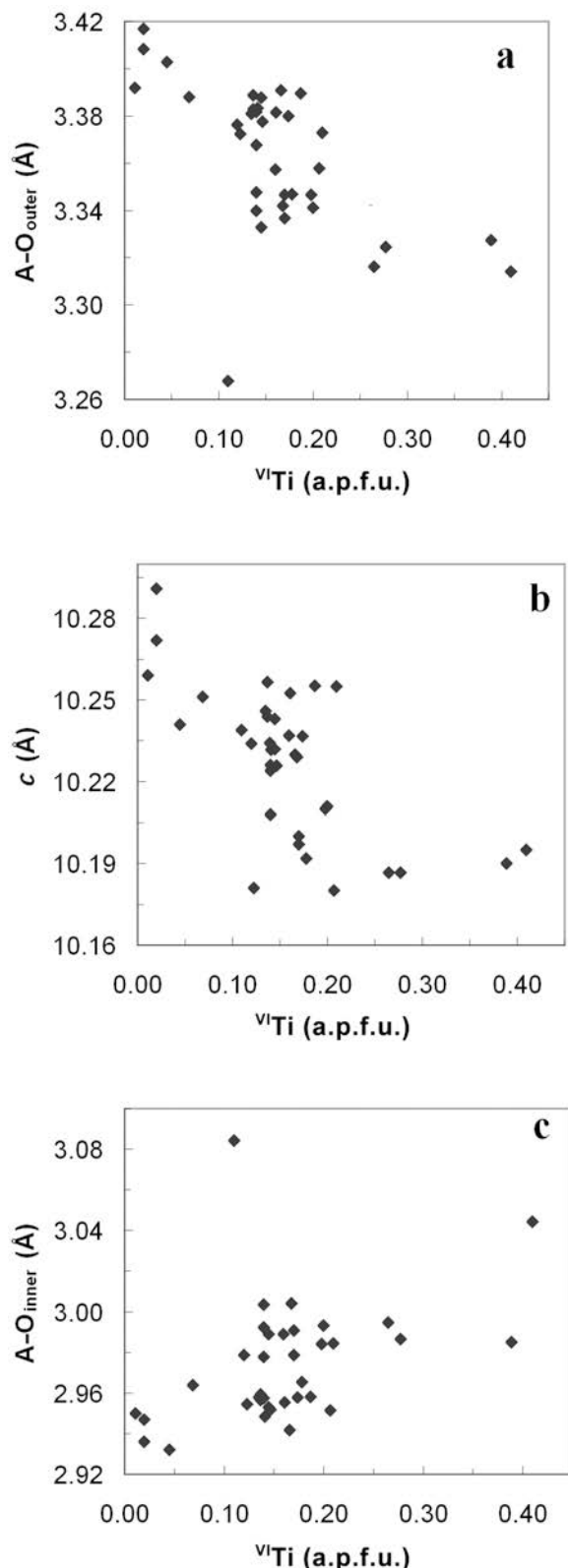


Figure 9. (a) ${}^{\text{VI}}\text{Ti}$ vs. $A-\text{O}_{\text{outer}}$, (b) the c axis, (c) $A-\text{O}_{\text{inner}}$.

Table 5) decrease the PBS value of the apical oxygen atom. Configurations that contain two or more adjacent octahedral vacancies are not physically reasonable.

To include bond-length considerations in the present modeling results, a bond-valence approach was implemented using the Brown (1992, eq. 5) bond-valence equation to calculate PBS values. However, the bond-valence equation requires observed bond lengths, and no bond-length data were available for the electrostatic models. Therefore, the variations in bond lengths and chemistry, as determined from the data set of phlogopite samples, were used to show the extremes in bond distances in these samples. The values for bond distances used were: $T-\text{O}_{\text{apical}} = 1.644\text{--}1.677 \text{ \AA}$ and $M-\text{O} = 2.005\text{--}2.113 \text{ \AA}$. Two most extreme cases were used to describe the chemical compositions: (1) maximum and minimum Al_{tot} content (${}^{\text{VI}}\text{Al}:{}^{\text{IV}}\text{Al}:\text{Vacancy} = 0.00:0.32:0.05$ to $0.21:0.33:0.03$ a.p.f.u.) and (2) independent ${}^{\text{VI}}\text{Al}$, ${}^{\text{IV}}\text{Al}$, and vacancy maximum and minima (${}^{\text{VI}}\text{Al}:{}^{\text{IV}}\text{Al}:\text{Vacancy} = 0.00:0.27:0.00$ to $0.21:0.35:0.10$ a.p.f.u.). Thus, this range is the variation in bond distance that is typically observed in structure refinements for Mg- and Al-rich phlogopites. The PBS was then calculated using the Brown equation and the determined minimum and maximum bond distances and two chemistry cases [case 1 and case 2 above]. In all cases, the PBS values from the models [case 1 = 1.936 to 1.991; case 2 = 1.925 to 2.020] fall within the extremes [case 1 = 1.870 to 2.353; case 2 = 1.850 to 2.421] using the minimum and maximum bond-distance values as described above and PBS summations as calculated from Brown. This result suggests that the structure can compensate for any charge imbalance by allowing bond distances to fall within the ranges derived from natural samples.

Limit of Al content in Al-rich phlogopite: other considerations

Hewitt and Wones (1975) suggested that the limit of Al substitution in trioctahedral biotites was determined by the limiting size of the interlayer site. As substitutions are made in the octahedral and tetrahedral sheets, the octahedral flattening angle (ψ) and tetrahedral rotation angle (α) are affected. In an ideal trioctahedral phlogopite with no substitutions, ψ is 54.73° and α is 0° , forming hexagonal tetrahedral rings, which create a twelve-coordinated interlayer site. Al cations substituted in tetrahedral sites cause an increase in lateral dimensions of the tetrahedral sheet, thus increasing α to minimize octahedral/tetrahedral misfit. In general, Al cations substituted in octahedral sites cause ψ to increase, the sheet to thin, and lateral dimensions to become smaller, also causing α to increase to minimize octahedral/tetrahedral misfit. As a result of the substitution, the interlayer coordination changes from twelve to six, to bring six basal oxygen atoms closer to the interlayer cation. $A-\text{O}$ bond lengths of $<\sim 2.8 \text{ \AA}$ were considered to be unstable (Hewitt and Wones, 1975), and

thus the size of the interlayer cation inhibits the amount of tetrahedral rotation allowed, which, in turn, controls the amount of Al that was substituted into the structure. This interpretation by Hewitt and Wones (1975) was later contested by Mercier *et al.* (2006), who found that the upper limit of tetrahedral rotation is 9.5° in near-IV^{IV}(AlSi₃) tetrahedral compositions. This upper limit was found to be determined by the tetrahedral sheets and not by the interlayer bond-length limits.

Natural Al-rich phlogopites have an octahedral VI^{VI}Al content ranging from 0.010 to 0.721 a.p.f.u., and the Al content is <1 a.p.f.u. for 1M polytypes (*C*2/*m* space group) (this study; Brigatti *et al.*, 2000; Brigatti and Poppi,

1993). As shown by Brigatti *et al.* (2003), Mercier *et al.* (2006), and this study, octahedral substitutions, especially Fe for Mg, affect structural (α , ψ , etc.) and topological (e.g. lateral cell parameters, *M*-*M* distances) parameters. For example, all the *M*-*M* octahedral distances (*i.e.* *M*1-*M*2 and *M*2-*M*2 distances) are affected by octahedral Al content (Figure 10a,b). The *M*1-*M*2 distances increase with octahedral Al content. Furthermore, a threshold value is observed for *M*2-*M*2 distances (at ~3.1 Å) at higher octahedral Al contents (Al³⁺ >0.35 a.p.f.u.). The sum of the *M*-*M* distances [*i.e.*, (*M*1-*M*2) + (*M*1-*M*2') + (*M*2-*M*2')], where *M*2' is the mirror equivalent of *M*2] should be ideally equal to the

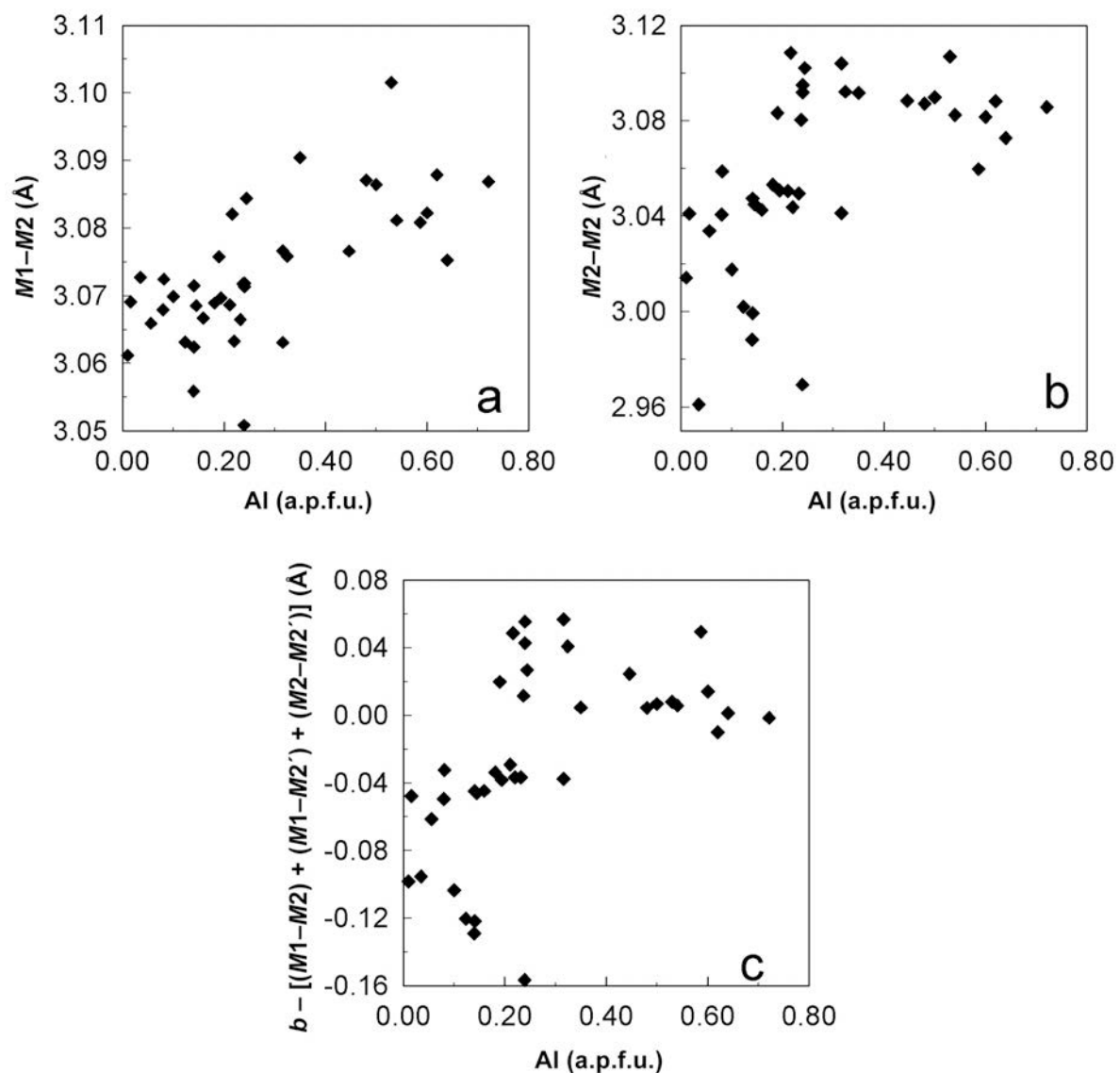


Figure 10. (a) *M*1 cation to *M*2 cation distance (Å), (b) *M*2 cation to *M*2' cation distance (Å) as a function of Al content (a.p.f.u.), and (c) the *b* cell parameter less the *M*1 to *M*2 cation distance, *M*1 to *M*2' cation distance, and the *M*2 to *M*2' cation distance as a function of Al content (a.p.f.u.). *M*2' indicates the mirror equivalent of *M*2.

lateral cell parameter b (Figure 10c). Where Al content increases, this sum approaches the size of the lateral b cell parameter, plus ~ 0.07 Å.

The modeling effort considered only electrostatic interactions of nearest neighbors to the M sites and not cation-cation interactions. No apparent evidence resulted from the modeling to indicate that electrostatic interactions contribute to limiting Al content in phlogopite. However, a possible limiting factor for octahedral Al substitution may be the relation between the $M-M$ distances and the lateral cell parameter, b , with changes in the latter mostly dependent on Fe-for-Mg substitution. Where Al content is $<0.3-0.4$ a.p.f.u., a linear relation is observed between octahedral cation distances and octahedral Al content. However, in contrast to the modeling, $M-M$ interactions probably involve shielding effects from electrostatic repulsions between the M cations. Thus, where octahedral Al content increases, a threshold value related to electrostatic repulsions between M cations is observed, although $M2-M2$ distances are probably more affected at smaller Al contents and $M1-M2$ distances at greater Al contents.

All evidence presented suggests that the Al content in the octahedral site may be limited by Fe-for-Mg substitutions to produce a lateral-cell (b) increase. This may suggest that a cation of lower charge substituting at $M1$ (or $M2$) may stabilize the structure at high Al contents, thus resulting in lower electrostatic repulsions between the octahedral sites. The latter mechanism may similarly affect trioctahedral micas with a low-charge $M1$ cation, such as Li-rich micas, and more extremely, dioctahedral micas.

ACKNOWLEDGMENTS

The authors thank C.V. Guidotti for providing the stimulus and samples for this study, Marty Yates, University of Maine, Orono, Maine, for the microprobe analysis, John T. Cheney for providing rock-sample information, and Sang Soo Lee for providing much initial guidance with the programming efforts. They are also grateful to Toshihiro Kogure, Giovanni Ferraris, Marcello Mellini, and an anonymous reviewer for their comments, and the Petroleum Research Fund of The American Chemical Society for partial funding under grant 43871-AC2.

REFERENCES

- Alietti, E., Brigatti, M.F., and Poppi, L. (1995) The crystal structure and chemistry of high-aluminum phlogopite. *Mineralogical Magazine*, **59**, 149–157.
- Bailey, S.W. (1984) Crystal chemistry of the true micas. Pp. 13–60 in: *Micas* (S.W. Bailey, editor). Reviews in Mineralogy, **13**, Mineralogical Society of America, Washington, D.C.
- Berman, R.G., Aranovich, L.Y., Rancourt, D.G., and Mercier, P.H. (2007) Reversed phase equilibrium constraints on the stability of Mg-Fe-Al biotite. *American Mineralogist*, **92**, 139–150.
- Brigatti, M.F. and Guggenheim, S. (2002) Mica crystal chemistry and the influence of pressure, temperature, and solid solution on atomistic models. Pp. 1–97 in: *Micas; Crystal Chemistry and Metamorphic Petrology* (A. Mottana, F.P. Sassi, J.B. Thompson, Jr., and S. Guggenheim, editors). *Reviews in Mineralogy and Geochemistry*, **46**. The Mineralogical Society of America, Chantilly, Virginia, and the Geochemical Society, St. Louis, Missouri, USA.
- Brigatti, M.F. and Poppi, L. (1993) Crystal chemistry of Ba-rich trioctahedral micas-1M. *European Journal of Mineralogy*, **5**, 857–871.
- Brigatti, M.F., Galli, E., and Poppi, L. (1991) Effect of Ti substitution in biotite-1M crystal chemistry. *American Mineralogist*, **76**, 1174–1183.
- Brigatti, M.F., Frigieri, P., Ghezzo, C., and Poppi, L. (2000) Crystal chemistry of Al-rich biotites coexisting with muscovites in peraluminous granites. *American Mineralogist*, **85**, 436–448.
- Brigatti, M.F., Guggenheim, S., and Poppi, M. (2003) Crystal chemistry of the 1M mica polytype: The octahedral sheet. *American Mineralogist*, **88**, 667–675.
- Brigatti, M.F., Caprilli, E., Funiciello, R., Giordano, G., Mottana, A., and Poppi, L. (2005) Crystal chemistry of ferroan phlogopites from the Albano maar lake (Colli Albani Volcano, central Italy). *European Journal of Mineralogy*, **17**, 611–621.
- Brigatti, M.F., Guidotti, C.V., and Malferrari, D. (2008) Single-crystal X-ray studies of trioctahedral micas coexisting with dioctahedral micas in metamorphic sequences from western Maine. *American Mineralogist*, **93**, 396–408.
- Brown, I.D. (1992) Chemical and Steric Constraints in Inorganic Solids. *Acta Crystallographica Section B – Structural Science*, **48**, 553–572.
- Bruker (2007) APEX2, GIS, SADABS and SAINT. Bruker AXS Inc., Madison, Wisconsin, USA.
- Burt, D.M. (1988) Vector representation of phyllosilicate compositions. Pp. 561–599 in: *Hydrous phyllosilicates (exclusive of micas)* (S.W. Bailey, editor). *Reviews in Mineralogy*, **19**, Mineralogical Society of America, Washington, D.C.
- Crowley, M.S. and Roy, R. (1964) Crystalline solubility in the muscovite and phlogopite groups. *American Mineralogist*, **49**, 348–362.
- Donnay, G., Donnay, J.D.H., and Takeda, H. (1964) Trioctahedral one-layer micas; Part 2, Prediction of the structure from composition and cell dimensions. *Acta Crystallographica*, **17**, 1374–1381.
- Guggenheim, S., Chang, Y., and Koster van Groos, A.F. (1987) Muscovite dehydroxylation; high-temperature studies. *American Mineralogist*, **72**, 537–550.
- Guidotti, C.V. (1974) Transition from staurolite to sillimanite zone, Rangeley Quadrangle, Maine. *Geological Society of America Bulletin*, **85**, 475–490.
- Guidotti, C.V. (1984) Micas in metamorphic rocks. Pp. 357–467 in: *Micas* (S.W. Bailey, editor). *Reviews in Mineralogy*, **13**, Mineralogical Society of America, Washington, D.C.
- Guidotti, C.V. and Dyar, M.D. (1991) Ferric iron in metamorphic biotite and its petrologic and crystallochemical implications. *American Mineralogist*, **76**, 161–175.
- Guidotti, C.V., Cheney, J.T., and Conatore, P.D. (1975) Coexisting cordierite + biotite + chlorite from the Rumford Quadrangle, Maine. *Geology (Boulder)*, **3**, 147–148.
- Guidotti, C.V., Cheney, J.T., and Henry, D.J. (1988) Compositional variation of biotite as a function of metamorphic reactions and mineral assemblage in the pelitic schists of western Maine. *American Journal of Science*, **288-A**, 270–292.
- Hewitt, D.A. and Wones, D.R. (1975) Physical properties of some synthetic Fe-Mg-Al trioctahedral biotites. *American Mineralogist*, **60**, 854–862.

- Laurora, A., Brigatti, M.F., Mottana, A., Malferrari, D., and Caprilli, E. (2007) Crystal chemistry of trioctahedral micas in alkaline and subalkaline volcanic rocks: a case study from Mt. Sassetto (Tolfa district, Latium, central Italy). *American Mineralogist*, **92**, 468–480.
- Lee, S.S., Guggenheim, S., Dyar, M.D., and Guidotti, C.V. (2007) Chemical composition, statistical analysis of the unit cell, and electrostatic modeling of the structure of Al-saturated chlorite from metamorphosed rocks. *American Mineralogist*, **92**, 954–965.
- Loewenstein, W. (1954) The distribution of aluminum in the tetrahedra of silicates and aluminates. *American Mineralogist*, **39**, 92–96.
- MathWorks (2006) *MatLab R2006b: The language of technical computing version 7*. Mathworks, Inc., Natick, Massachusetts, USA.
- Mercier, P.H.J., Rancourt, D.G., and Redhammer, G.J. (2006) Upper limit of the tetrahedral rotation angle and factors affecting octahedral flattening in synthetic and natural $1M$ polytype $C2/m$ space group micas. *American Mineralogist*, **91**, 831–849.
- Ohta, T., Takeda, H., and Takeuchi, Y. (1982) Mica polytypism; similarities in the crystal structures of coexisting $1M$ and $2M_1$ oxybiotite. *American Mineralogist*, **67**, 298–310.
- Robert, J.L. (1976) Phlogopite solid solutions in the system $K_2O\text{-MgO}\text{-Al}_2O_3\text{-SiO}_2\text{-H}_2O$. *Chemical Geology*, **17**, 195–212.
- Robinson, K., Gibbs, G.V., and Ribbe, P.H. (1971) Quadratic elongation: A quantitative measure of distortion in coordination polyhedra. *Science*, **172**, 567–570.
- Rutherford, M.J. (1973) The phase relations of aluminous iron biotites in the system $KAlSi_3O_8\text{-KAlSiO}_4\text{-Al}_2O_3\text{-Fe-O-H}$. *Journal of Petrology*, **14**, 159–178.
- Schingaro, E., Scordari, F., Mesto, E., Brigatti, M.F., and Pedrazzi, G. (2005) Cation-site partitioning in Ti-rich micas from Black Hill (Australia); a multi-technical approach. *Clays and Clay Minerals*, **53**, 179–189.
- Shannon, R.D. (1976) Revised effective ionic-radii and systematic studies of interatomic distances in halides and chalcogenides. *Acta Crystallographica Section A*, **32**, 751–767.
- Sheldrick, G.M. (1997) *SHELXTL97 version 5.1: Program for the Solution and Refinement of Crystal Structures*. University of Göttingen, Germany.

(Received 5 June 2008; revised 22 May 2009; Ms. 168; A.E. T. Kogure)